

Experimental Compliance Matrix Derivation for Enhancing Trajectory Tracking of a 2-DoF High-Accelerated Over-Constrained Mechanism

Erkan Paksoy¹, M. İ. Can Dede¹, and Gökhan Kiper¹

Izmir Institute of Technology, Izmir, Turkey,
erkanpaksoy, candede, gokhankiper@iyte.edu.tr

Abstract. If the positioning accuracy of the end-effector of a robot has high priority, compliance characteristics of the elements of its mechanism should be considered. Due to the external loading on the robot, the dimensions of the elements change and this leads to positioning errors for the end-effector. In this paper, an experimental test setup and an experimental procedure are described to derive the compliance characteristics of a planar 2-degree-of-freedom mechanism.

Keywords: Positioning Accuracy, Parallel Mechanism, Experimental Compliance Matrix Derivation

1 Introduction

In order to express the positioning performance of a robotic manipulator, commonly the resolution, repeatability and accuracy of the robot are considered. The resolution is defined as the smallest incremental step that the robot's end-effector can move, and it mostly depends on the actuator and sensor capabilities. Repeatability is defined as the robot's ability to return to the same position and orientation. Accuracy is a measure of how accurately the robot can move to a desired location in the workspace [2].

Factors that affect the accuracy of a robotic manipulator named as inaccuracy factors and classified into two groups as geometrical errors and non-geometrical errors. Geometrical errors are due to three factors: manufacturing tolerances, assembly process and joint clearance. On the other hand, non-geometrical errors can be categorized into 5 subgroups which are compliance errors, measurement errors, environmental factors (temperature, humidity), control errors and the final one is the problems caused in the joint structure: friction, backlash and wear [6].

All 3 subgroups in the geometrical factors affect the accuracy of the robot and joint clearance errors have a dominant effect on the repeatability of the robot. By various calibration methods, the accuracy problems can be solved. To enhance the repeatability of a robot, an over-constrained kinematic structure can be used so that the effect of the joint clearances is reduced. Over-constrained mechanisms

have lower computed degrees of freedom (DoF) than practical degrees of freedom [3].

In this paper, we want to focus on how compliance information of the end-effector point can be obtained for a 2-DoF over-constrained planar parallel manipulator. Here, we assume that the other non-geometrical factors have small effect on the end-effector position compared to the effect of the compliance errors. The reason of assuming compliance errors have dominant effect on the end-effector location is that the mechanism includes links manufactured as a combination of aluminum parts and carbon fiber tubes connected to each other by glue and the end-effector accelerations are up to 5g.

In order to determine the Cartesian compliance matrix or stiffness matrix of the manipulator, there are two methods classified as analytical and experimental stiffness modeling methods. In this paper, an experimental stiffness modeling method is described and the results of the experiments are presented for a 2-DoF over-constrained planar mechanism.

In experimental stiffness evaluation systems, generally the system consists of 2 elements; one of them is the displacement measurement sensor and the other one is the calibrated masses to create different set of force matrices. In an example experimental method, a formulation for numerical and experimental stiffness analysis and basic principles on how the stiffness matrix of a manipulator can be obtained experimentally are given. In a previous study, an experimental stiffness measuring system called Milli-CATRASYs system was produced to procure the stiffness characteristics of a parallel manipulator called CaPaMan. This system includes LVDT sensors on the steel wires in order to measure the end-effector displacements and calibrated masses on the end of each wire to create different set of force matrices [1].

In another experimental stiffness measurement method, a measurement system composed of cameras is used to measure the end-effector displacements of a haptic device [7].

In [4], for experimental validation of the analytical stiffness model of the R-CUBE mechanism, a test setup combined of a laser range sensor and a pulley-guide system is used.

In this paper, Faro Prime Measuring Arm 1.2 is used as the displacement measuring element and calibrated weights are used via a wire-pulley system to create different forces at the end-effector of a 2-DoF over-constrained mechanism designed for planar laser marking operation with high acceleration motion capability. The aim of this paper is to obtain compliant displacements of the center of gravity (CG) of the end-effector by applying a variety of forces at various locations of its workspace.

2 2-DoF Planar Over-constrained Mechanism

The two mechanisms presented in Fig. 1.a and 1.b are kinematically equivalent when the positioning of point C is of concern given that the corresponding link lengths are equal to each other. An extensive description of this kinematic equivalence is presented in [5]. The advantage of having an over-constrained

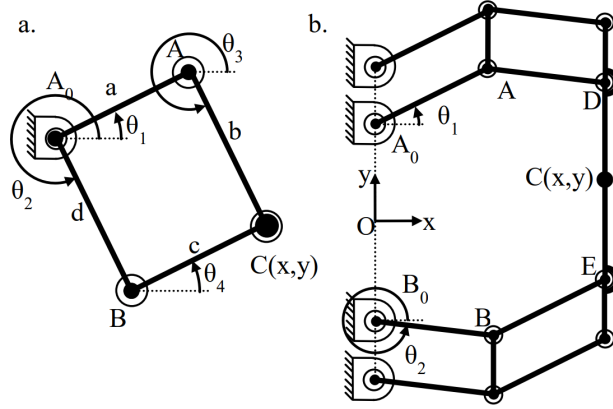


Fig. 1. a) 5R Mechanism, b) 6R Over-constrained mechanism [5]

mechanism is to have better repeatability and enhanced stiffness performance. However, for the mechanism in Fig.1b, there is no analytical inverse kinematics solution. For calibration and control purposes, the inverse kinematics of hidden robot model given in Fig.1a can be used.

In Fig. 2, CAD model of the over-constrained mechanism is illustrated and important components of the mechanism are explained.

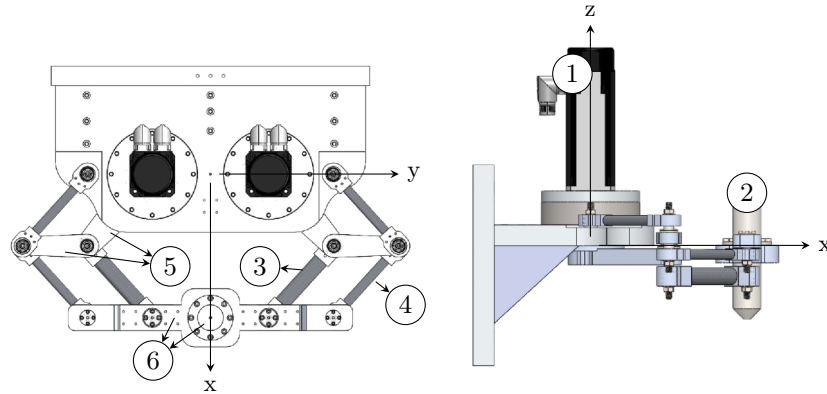


Fig. 2. a) Top-view of the 3D Model, b) Right-view of the 3D model; 1: motor and reducers, 2: Replica of the laser-head end-effector, 3: Thick distal links, 4: Thin links, 5: Aluminum Links, 6: Platform including end-effector

In the following, position level forward kinematics of hidden robot model is given:

$$\left| \overrightarrow{A_0A} \right| = \left| \overrightarrow{A_0B} \right| = \left| \overrightarrow{AC} \right| = \left| \overrightarrow{BC} \right| = l = 150 \text{ mm} \quad (1)$$

Because of the parallelogram loops; $\theta_1 = \theta_4, \theta_2 = \theta_3$ (2)

$$\vec{r}_c = \vec{A_0A} + \vec{AC} = \vec{A_0B} + \vec{BC} = l(e^{i\theta_1} + e^{i\theta_3}) = l(e^{i\theta_2} + e^{i\theta_4}) \quad (3)$$

By using (2) in (3); $\vec{r}_c = l(e^{i\theta_1} + e^{i\theta_2})$ (4)

By simplifying (4); $x = l[\cos(\theta_1) + \cos(\theta_2)], y = l[\sin(\theta_1) + \sin(\theta_2)]$ (5)

3 Experimental Setup

In Fig. 3, the experimental test setup to measure the compliant displacement of the end-effector is given. To measure the compliant displacement of the end-effector point of the mechanism Faro Prime Arm ($\pm 23 \mu m$ measurement accuracy) is used and to exert a force at any point in the workspace of the mechanism,

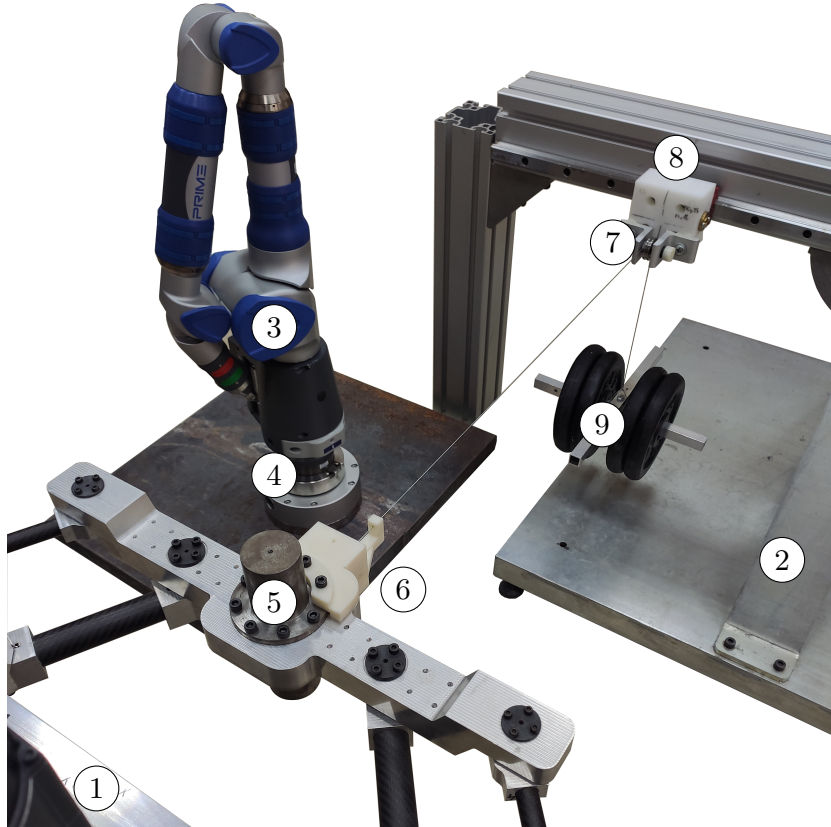


Fig. 3. Experimental Test Setup; 1: 2-DoF planar mechanism, 2: Translational mechanism to arrange the force direction, 3: Faro Prime Arm, 4: Magnetic base, 5: Replica of laser head, 6: Guide, 7: Pulley, 8: Linear rail, 9: Calibrated weight

a system that includes a 3D translational mechanism, calibrated weight and steel wire is used. Faro Prime Arm is fixed to a 60 kg metal sheet by using a magnetic base ensures that the location of the Faro Prime Arm does not change while taking measurements. The center of gravity of the replica of the laser-head end-effector and the guide details are given in Fig. 4. For clarity, the CG of the end-effector is defined with respect to the whole moving platform including end-effector (see Fig. 2). Compliant displacement measurements at the CG can change with respect to mainly two factors. These factors are the a) measurement point on the mechanism, b) the force vector \vec{F} .

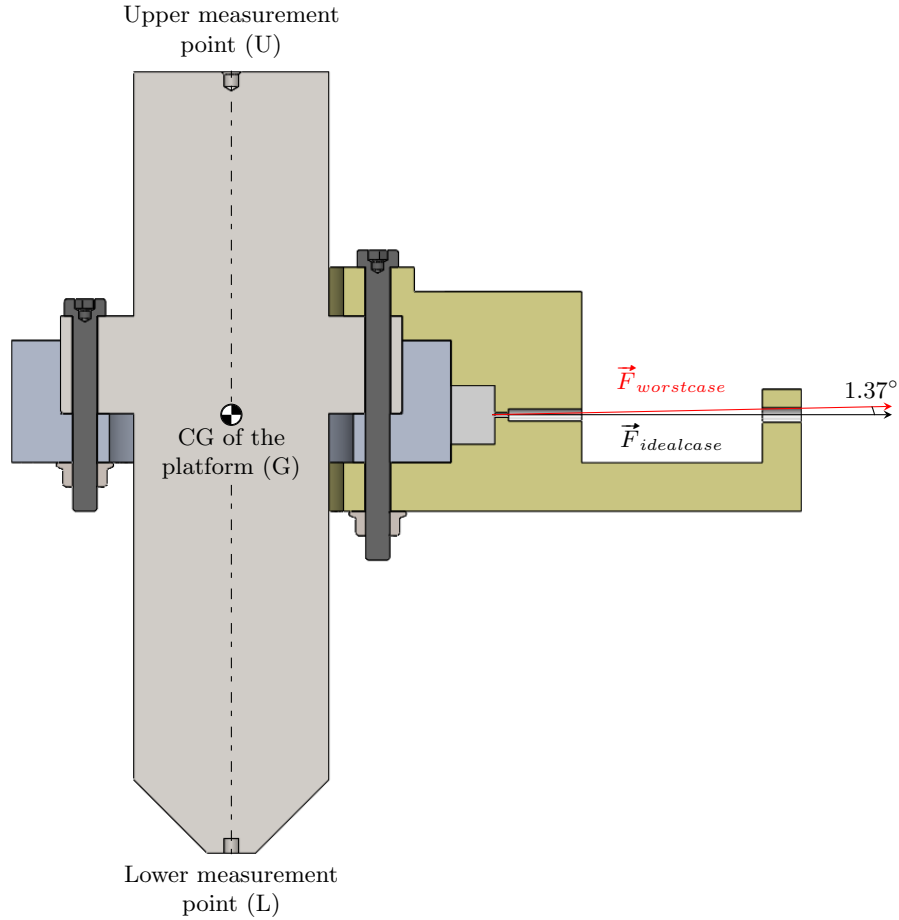


Fig. 4. Replica of laser head and guide details: $|\vec{UG}| = 69$ mm, $|\vec{UL}| = 160$ mm

To acquire the compliant displacements at the CG of the platform as a 6-DoF information (3 translational displacements and 3 angular displacements), replica of the laser-head that contains 2 measurement points is designed and located at the end-effector of the mechanism (Fig. 4). By using \vec{UL} information

presented in Fig. 4, compliance displacements at any point along the vertical-axis for the end-effector of the mechanism can be derived. In this way, we can calculate the positional deviation of the laser beam on the workpiece. Since the distance between the laser head and the workpiece can change with respect to the material, laser power and the thickness of the workpiece, in this study, we used the CG point for our calculations. To obtain repeatable tests, calibrated masses are used to generate the magnitude of the exerted force at the end-effector. The direction of the external force is regulated by the use of a guide that is presented in Fig. 4. The steel wire goes through the cylindrical hole ensures that the maximum deviation of force direction is 1.37° . That means, 99.97% of the loading will be in the desired direction if we neglect compliance of the mechanism because of the small forcing along other directions.

4 Experimental Procedure

The coordinate system of the robot is located between the two motors and the operational workspace of the robot is determined as 150 mm x 100 mm. In Fig. 5, the coordinate system of the robot and 15 measurement points on the workspace are given.

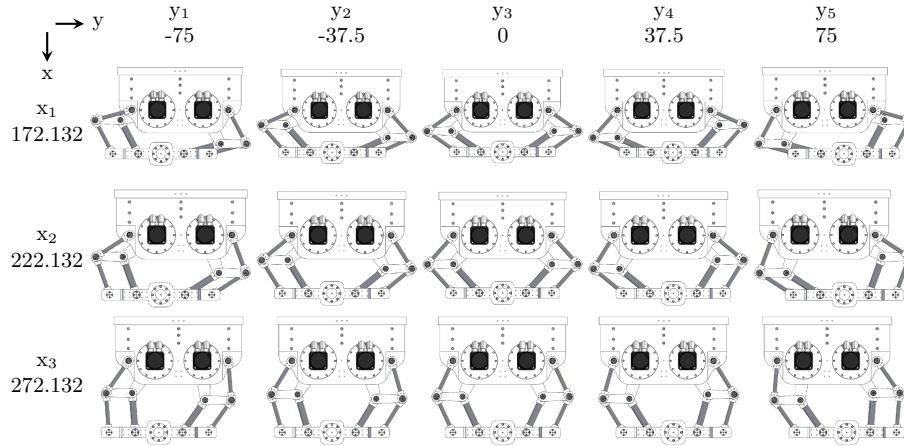


Fig. 5. Mechanism configurations and end-effector locations given in mm for the measurement points

At all measurement points of the workspace, the applied external forces are defined in steps in Table 1. In Step 0, there is a small amount of force because of the steel wire system. In each step, approximately 5 kg mass is added to system to exert a force and then, the coordinates of the upper measurement point (U) and Lower Measurement Point (L) are measured and recorded (Fig. 4).

To determine the location of CG of the platform (G) Equations 6, 7 and 8 are used. If \vec{UL} is known for each step, then both translational and angular compliant displacements of the platform can be found.

Table 1. Applied external force at each test step

Step	Exerted Force (kgf) \approx in (N)	
0	0.11	0
1	5	50
2	9.92	100
3	14.89	150
4	19.83	200
5	24.86	250

$$\vec{U} = U_x \vec{i} + U_y \vec{j} + U_z \vec{k}, \vec{L} = L_x \vec{i} + L_y \vec{j} + L_z \vec{k} \quad (6)$$

$$\overline{UL} = (L_x - U_x) \vec{i} + (L_y - U_y) \vec{j} + (L_z - U_z) \vec{k} \quad (7)$$

$$\vec{G} = \vec{U} + \frac{69}{160} \overline{UL} \quad (8)$$

5 Test Results

In Table 2, the translational compliant displacements under the forces (50-250 N) along +X direction are given. As it was expected, because of the symmetrical structure of the mechanism, there are no ΔY displacement for the points that are located on +X-axis ($Y = 0$ mm) while the forces are increasing at +X-direction.

Table 2. Compliant displacements of CG under the forces in +X-direction (mm)

\vec{F} in \vec{X}	ΔX	ΔY	ΔZ	ΔX	ΔY	ΔZ	ΔX	ΔY	ΔZ	ΔX	ΔY	ΔZ	ΔX	ΔY	ΔZ
	x_1y_1 (172.132, -75)			x_1y_2 (172.132, -37.5)			x_1y_3 (172.132, 0)			x_1y_4 (172.132, 37.5)			x_1y_5 (172.132, 75)		
50 N	0.105	0.061	-0.031	0.035	0.027	-0.009	0.027	0.002	-0.011	0.044	-0.024	-0.017	0.088	-0.058	-0.022
100 N	0.198	0.109	-0.039	0.085	0.047	-0.016	0.059	0.002	-0.018	0.091	-0.040	-0.028	0.182	-0.094	-0.028
150 N	0.289	0.164	-0.046	0.132	0.068	-0.030	0.094	0.000	-0.044	0.137	-0.059	-0.045	0.279	-0.151	-0.047
200 N	0.389	0.205	-0.060	0.180	0.080	-0.051	0.129	-0.006	-0.056	0.184	-0.077	-0.057	0.369	-0.190	-0.055
250 N	0.479	0.257	-0.080	0.226	0.096	-0.065	0.164	-0.009	-0.067	0.231	-0.099	-0.066	0.462	-0.232	-0.070
	x_2y_1 (222.132, -75)			x_2y_2 (222.132, -37.5)			x_2y_3 (222.132, 0)			x_2y_4 (222.132, 37.5)			x_2y_5 (222.132, 75)		
	50 N	0.045	0.039	-0.020	0.027	0.019	0.008	0.024	-0.003	-0.023	0.027	-0.014	-0.012	0.044	-0.042
100 N	0.085	0.083	-0.031	0.054	0.036	-0.021	0.054	-0.005	-0.041	0.058	-0.026	-0.030	0.089	-0.084	-0.041
150 N	0.131	0.118	-0.051	0.087	0.048	-0.026	0.083	-0.001	-0.059	0.091	-0.041	-0.031	0.133	-0.126	-0.054
200 N	0.176	0.151	-0.073	0.120	0.062	-0.047	0.111	0.007	-0.068	0.118	-0.056	-0.048	0.178	-0.153	-0.064
250 N	0.218	0.201	-0.081	0.147	0.077	-0.064	0.140	0.002	-0.079	0.147	-0.074	-0.070	0.220	-0.200	-0.091
	x_3y_1 (272.132, -75)			x_3y_2 (272.132, -37.5)			x_3y_3 (272.132, 0)			x_3y_4 (272.132, 37.5)			x_3y_5 (272.132, 75)		
	50 N	0.039	0.088	-0.023	0.022	0.027	-0.023	0.012	0.002	-0.016	0.020	-0.029	-0.016	0.039	-0.085
100 N	0.084	0.181	-0.052	0.050	0.070	-0.035	0.031	0.001	-0.030	0.043	-0.064	-0.037	0.084	-0.175	-0.041
150 N	0.124	0.275	-0.054	0.075	0.104	-0.070	0.048	0.000	-0.055	0.068	-0.101	-0.061	0.128	-0.270	-0.065
200 N	0.170	0.359	-0.077	0.098	0.138	-0.087	0.071	-0.006	-0.079	0.094	-0.140	-0.080	0.167	-0.348	-0.082
250 N	0.209	0.447	-0.104	0.117	0.175	-0.105	0.094	-0.003	-0.096	0.114	-0.164	-0.090	0.208	-0.430	-0.107

Also, absolute magnitudes of the translational displacement values are found to be symmetrical with respect to the +X-axis taking into account the resolution of the measurement system. These two observations are obtained from the measurement results to verify the test procedure's suitability.

Moreover, while forces are increasing linearly along $+X$ -direction 50 N to 250 N, the displacements are also increasing linearly. For instance, the displacement values for the measurement point (172.123, -75) are increasing linearly as the external force is increased linearly (0.1 mm for 50 N, 0.2 mm for 100 N, etc.). These results suggest that for each point there is almost a linear relationship between the external force and compliant displacements along at the X - and Y -directions.

Table 3. Compliant displacements of CG under the forces in $-Y$ -direction (mm)

\vec{F} in $-\vec{Y}$	ΔX	ΔY	ΔZ	ΔX	ΔY	ΔZ	ΔX	ΔY	ΔZ	ΔX	ΔY	ΔZ	ΔX	ΔY	ΔZ
	x_1y_1 (172.132, -75)			x_1y_2 (172.132, -37.5)			x_1y_3 (172.132, 0)			x_1y_4 (172.132, 37.5)			x_1y_5 (172.132, 75)		
50 N	-0.069	-0.079	-0.006	-0.026	-0.091	-0.001	-0.003	-0.084	0.006	0.022	-0.078	-0.003	0.054	-0.086	0.007
100 N	-0.110	-0.190	-0.007	-0.047	-0.182	0.003	0.002	-0.172	0.008	0.051	-0.168	0.017	0.113	-0.182	0.016
150 N	-0.177	-0.283	-0.012	-0.074	-0.268	0.002	-0.013	-0.246	0.006	0.071	-0.256	0.005	0.160	-0.273	0.012
200 N	-0.243	-0.374	-0.019	-0.090	-0.357	0.001	-0.020	-0.326	0.010	0.088	-0.335	0.007	0.216	-0.359	0.013
250 N	-0.309	-0.473	-0.033	-0.115	-0.449	0.001	-0.019	-0.420	0.005	0.117	-0.434	0.019	0.266	-0.449	0.015
	x_2y_1 (222.132, -75)			x_2y_2 (222.132, -37.5)			x_2y_3 (222.132, 0)			x_2y_4 (222.132, 37.5)			x_2y_5 (222.132, 75)		
50 N	-0.033	-0.133	-0.005	-0.031	-0.115	-0.009	-0.004	-0.110	0.004	0.020	-0.120	0.000	0.055	-0.122	0.011
100 N	-0.078	-0.258	-0.009	-0.040	-0.243	-0.006	0.001	-0.232	0.006	0.050	-0.236	0.006	0.087	-0.251	0.013
150 N	-0.114	-0.384	-0.015	-0.063	-0.366	-0.006	0.004	-0.357	0.013	0.065	-0.358	0.008	0.129	-0.375	0.021
200 N	-0.161	-0.509	-0.008	-0.077	-0.488	-0.012	0.002	-0.475	0.014	0.083	-0.473	0.000	0.174	-0.499	0.014
250 N	-0.204	-0.638	-0.016	-0.099	-0.609	-0.006	0.009	-0.604	0.009	0.099	-0.593	0.005	0.205	-0.628	0.014
	x_3y_1 (272.132, -75)			x_3y_2 (272.132, -37.5)			x_3y_3 (272.132, 0)			x_3y_4 (272.132, 37.5)			x_3y_5 (272.132, 75)		
50 N	-0.061	-0.346	-0.004	-0.039	-0.265	-0.009	-0.002	-0.246	0.000	0.038	-0.255	0.001	0.098	-0.319	0.000
100 N	-0.148	-0.685	-0.009	-0.071	-0.532	-0.010	0.009	-0.494	-0.023	0.077	-0.523	-0.005	0.193	-0.658	-0.010
150 N	-0.261	-1.001	-0.026	-0.105	-0.789	-0.014	0.013	-0.755	-0.014	0.118	-0.792	-0.002	0.275	-0.998	-0.005
200 N	-0.335	-1.349	-0.023	-0.140	-1.052	-0.015	0.003	-0.990	-0.014	0.155	-1.042	0.004	0.358	-1.331	-0.012
250 N	-0.421	-1.690	-0.028	-0.182	-1.319	-0.016	0.011	-1.251	-0.008	0.195	-1.305	0.002	0.458	-1.671	-0.009

In Table 3, the translational compliant displacements under the forces (50-250N) along $-Y$ -direction are given. This time, due to the symmetry there are no ΔX displacement at the $+X$ -axis while the external load is applied $-Y$ -direction. The symmetrical compliant displacement magnitudes with respect to the $+X$ -axis are obtained and almost a linear relationship can be seen again.

6 Conclusion

As a result of this work, the compliance behavior of a 2-DoF planar over-constrained mechanism is gathered by using a test setup including Faro Prime arm as coordinate-measurement machine and a combination of 3D translational mechanism and steel-wire equipment as external force application system. This compliance information will be used in future studies to improve the positioning accuracy of the 2-DoF planar over-constrained mechanism during high acceleration (up to 5 g) operation.

Acknowledgement. The study is supported in part by The Scientific and Technological Research Council of Turkey via grant number 116M272. We thank Dr. Emre Uzunoğlu and Mr. İbrahimcan Görgülü, who contributed to the design of the experimental test setup.

References

1. Ceccarelli, M., Carbone, G.: Numerical and experimental analysis of the stiffness performances of parallel manipulators. In: 2nd international colloquium collaborative research centre. vol. 562, pp. 21–35. Citeseer (2005)
2. Conrad, K.L., Shiakolas, P.S., Yih, T.: Robotic calibration issues: Accuracy, repeatability and calibration. In: Proceedings of the 8th Mediterranean Conference on Control and Automation (MED2000), Rio, Patras, Greece. vol. 1719 (2000)
3. Gogu, G.: Mobility of mechanisms: a critical review. *Mechanism and Machine Theory* 40(9), 1068–1097 (2005)
4. Görgülü, İ., Dede, M.C., Carbone, G.: An experimental test procedure for validation of stiffness model: A case study for r-cube parallel mechanism. In: IFToMM International Symposium on Robotics and Mechatronics. pp. 391–402. Springer (2019)
5. Kiper, G., Dede, M.İ.C., Uzunoğlu, E., Mastar, E.: Use of hidden robot concept for calibration of an over-constrained mechanism (2015)
6. Klimchik, A.: Enhanced stiffness modeling of serial and parallel manipulators for robotic-based processing of high performance materials. Ph.D. thesis, Ecole Centrale de Nantes (ECN); Ecole des Mines de Nantes (2011)
7. Taner, B., Dede, M.İ.C.: Image processing based stiffness mapping of a haptic device. In: *New Advances in Mechanisms, Mechanical Transmissions and Robotics*, pp. 447–454. Springer (2017)